6 DISCUSSION

In the thirty years since the seminal experiment by Christenson *et al.* [Chr 70], the Drell-Yan process for continuum dilepton production in hadronic interactions remains an active area of experimental and theoretical investigation. Several experiments have studied both pion- and proton-induced dileptons, providing a wealth of data utilizing various beams, targets and center-of-mass energies. When these data are analyzed within the framework of perturbative QCD along with data from other types of hadronic interactions, they provide a powerful tool for extracting information about the parton distribution functions.

In the preceding chapters we have described the procedures used in and reported the results of a measurement of continuum diumon cross sections in 800-GeV pp and pd interactions. In this chapter, we compare our results to existing dimuon data from pA and pd measurements performed by the CERN NA3 [Bad 83], FNAL E605 [Mor 91] and FNAL E772 [McG 94] experiments. Fermilab E866 has already published [Haw 98, Tow 01] results on the deuterium-to-hydrogen cross section ratio, and we will also demonstrate that our absolute measurements are consistent with those previous results. We will also discuss the level of agreement between our results and next-to-leading order calculations of the cross sections based on various sets of parton distribution fits. We will highlight some important differences between data and theory, and discuss the likely impact our results will have on future fits to the parton distributions.

6.1 Comparison with Other Experiments

Following the work of Christenson *et al.*, several experiments measured Drell-Yan cross sections using various beams and targets. The first high-statistics measurements to study the Drell-Yan process over an extended range of kinematics examined dimuon production in pA interactions. CERN NA3 [Bad 83] studied pPt at $\sqrt{s} = 27.4$ GeV, while Fermilab E605 [Mor 91] studied pCu at $\sqrt{s} = 38.8$ GeV. Less extensive measurements of the pp and pd cross sections in a narrow x_F range centered around $x_F = 0$ were also carried out at CERN. CERN R-209 [Ant 82] studied the pp cross sections at $\sqrt{s} = 44$ and 62 GeV, while CERN NA51 [Bal 94] studied the pp and pd cross sections[1] at $\sqrt{s} = 29$ GeV. In the early 1990's, the pd cross sections were measured over a wide range of mass and x_F by the Fermilab E772 collaboration [McG 94]. They published results spanning the range $0.05 \leq x_F \leq 0.7$ based on an $83,000$ event dimuon sample. It is important to note that the E605 and E772 measurements were conducted using essentially the same apparatus as E866. Thus, these two experiments provide important cross checks on the consistency of our results.

Figures 6.1 and 6.2 compare the E866 measurements of the scaling form of

[1] CERN NA51 did not publish absolute measurements, only the asymmetry between pp and pd cross sections.

the cross section $M^3 d^2\sigma/dM dx_F$ in pd interactions to the NA3, E605 and E772 measurements. The data are plotted versus the scaling variable $\sqrt{\tau}$ to enable a direct comparison between the results measured at different $\sqrt{s}$. The E866 data, which are subject to an additional $\pm 6.5\%$ global normalization uncertainty, are in good agreement with these previous dimuon experiments over a broad range of mass and x_F. The E605, E772 and E866 data typically agree to within less than the quoted normalization uncertainties[2] of the three experiments. The only major area of disagreement is at larger values of x_F and smaller masses, where the E866 measurement differs significantly from the E772 results. In this kinematic region, the E772 measurement is subject to larger systematic uncertainties ($\sim 20\%$) [?]. The major differences between E772 and E866 in this region are thought to be primarily due to uncertainties in the E772 magnetic field maps [McG].

Because the E772 and E866 measurements used essentially the same apparatus it is worth exploring this difference in a little more detail. Figure 6.3 shows the results from the low- and high-mass data settings used in E866, and the published E772 results. They are shown over the range $0.4 \leq x_F < 0.5$ where the discrepancy is most pronounced. The two E866 mass settings have very different acceptances. The acceptance in the high-mass data is plunging rapidly with decreasing mass, while the low-mass acceptance is fairly large in the same region. The agreement

[2] We expect the systematic uncertainties in the normalization of these three experiments to be correlated at some level, since they used the same beam line monitors to calibrate the data, and some of the same calibration measurements are common.

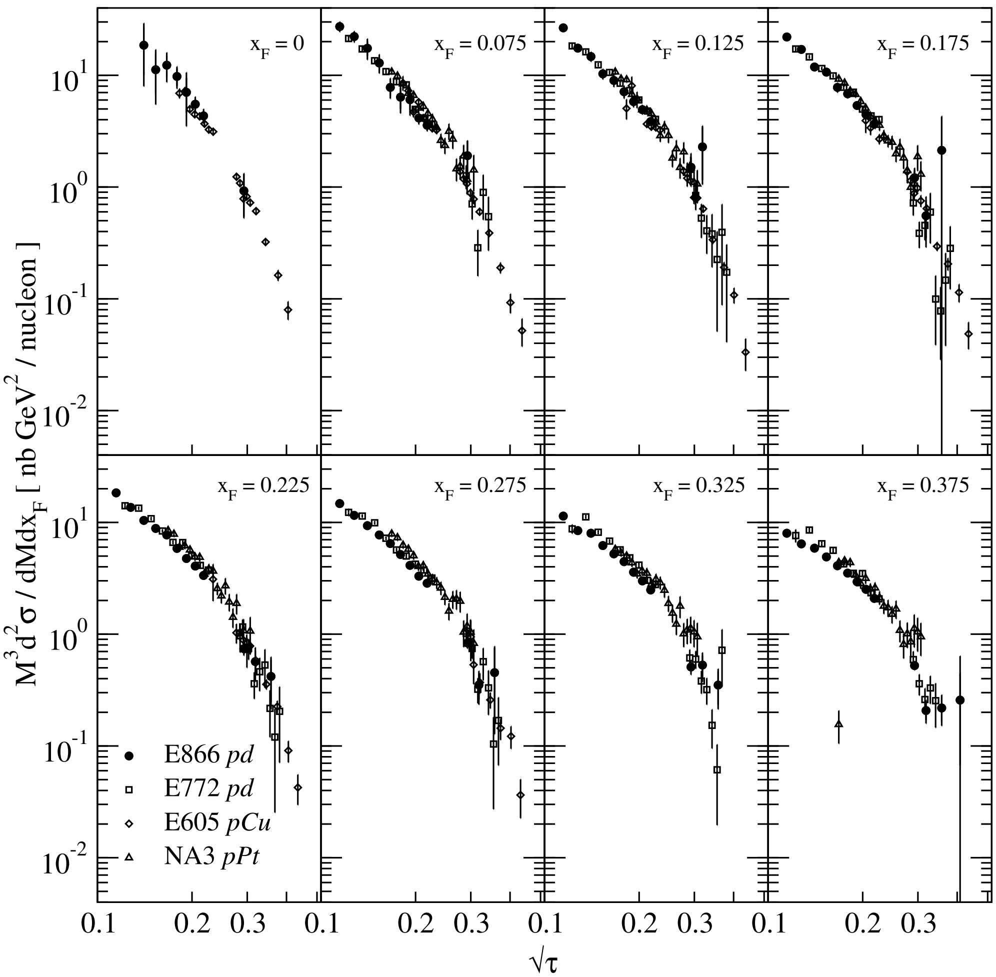

Figure 6.1: Scaling form $M^3 d^2\sigma/dM\,dx_F$ plotted versus $\sqrt{\tau}$ for the E866 pd, E772 pd [McG 94], E605 pCu [Mor 91] and NA3 pPt [Bad 83] measurements. Errors are statistical only, except for the E866 uncertainties which are the linear sum of statistical and systematic uncertainties. The E866 data contain an additional $\pm 6.5\%$ systematic uncertainty in the normalization.

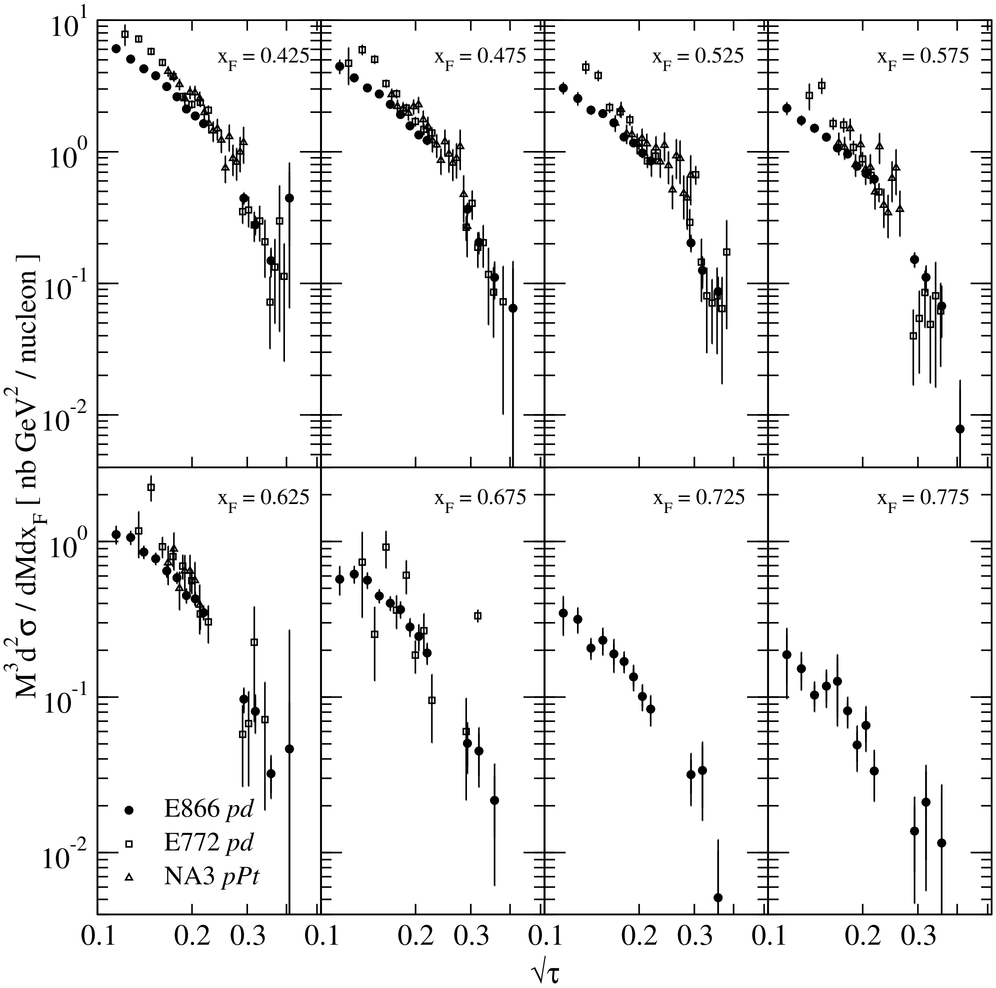

Figure 6.2: Scaling form $M^3 d^2\sigma/dM dx_F$ plotted versus $\sqrt{\tau}$ for the E866 pd, E772 pd [McG 94], and NA3 pPt [Bad 83] measurements. Errors are statistical only, except for the E866 uncertainties which are the linear sum of the statistical and systematic uncertainties. The E866 data contain an additional $\pm 6.5\%$ systematic uncertainty in the normalization.

between these data sets is quite good, suggesting that the E866 data is generally free of the systematic uncertainties present in the E772 data in this region.

Fermilab E772 has also published measurements of the triple-differential cross section $Ed^3\sigma/dp^3$, over a more restricted kinematic range ($0.1 \leq x_F \leq 0.3$) than their double-differential measurements. This range is below the x_F range where the E772 and E866 measurements disagree, and was imposed on E772 by correlations between their x_F and p_T acceptance [McG], which was much less of a concern in the E866 data. In the previous chapter we tabulated $Ed^3\sigma/dp^3$ in various x_F bins covering our entire x_F range. To make a direct comparison between our results and those of E772, we recalculated our cross sections using the E772 binning. These results are shown in figure 6.4 along with the E772 measurement. In general, there is excellent agreement between the two experiments. Only as $p_T \to 0$ GeV do the two experiments disagree. The cross sections in this region are highly sensitive to the precise alignment of the beam. Uncertainties in either or both the beam position and angle would lead to systematic shifts in the p_T of each event. Thus, the differences between the two measurements may be due to beam alignment issues in the two experiments.

6.2 Cross Section Ratios

We turn now to a comparison of our absolute measurements with the previously published cross section ratios. The primary goal of Fermilab E866 was to measure

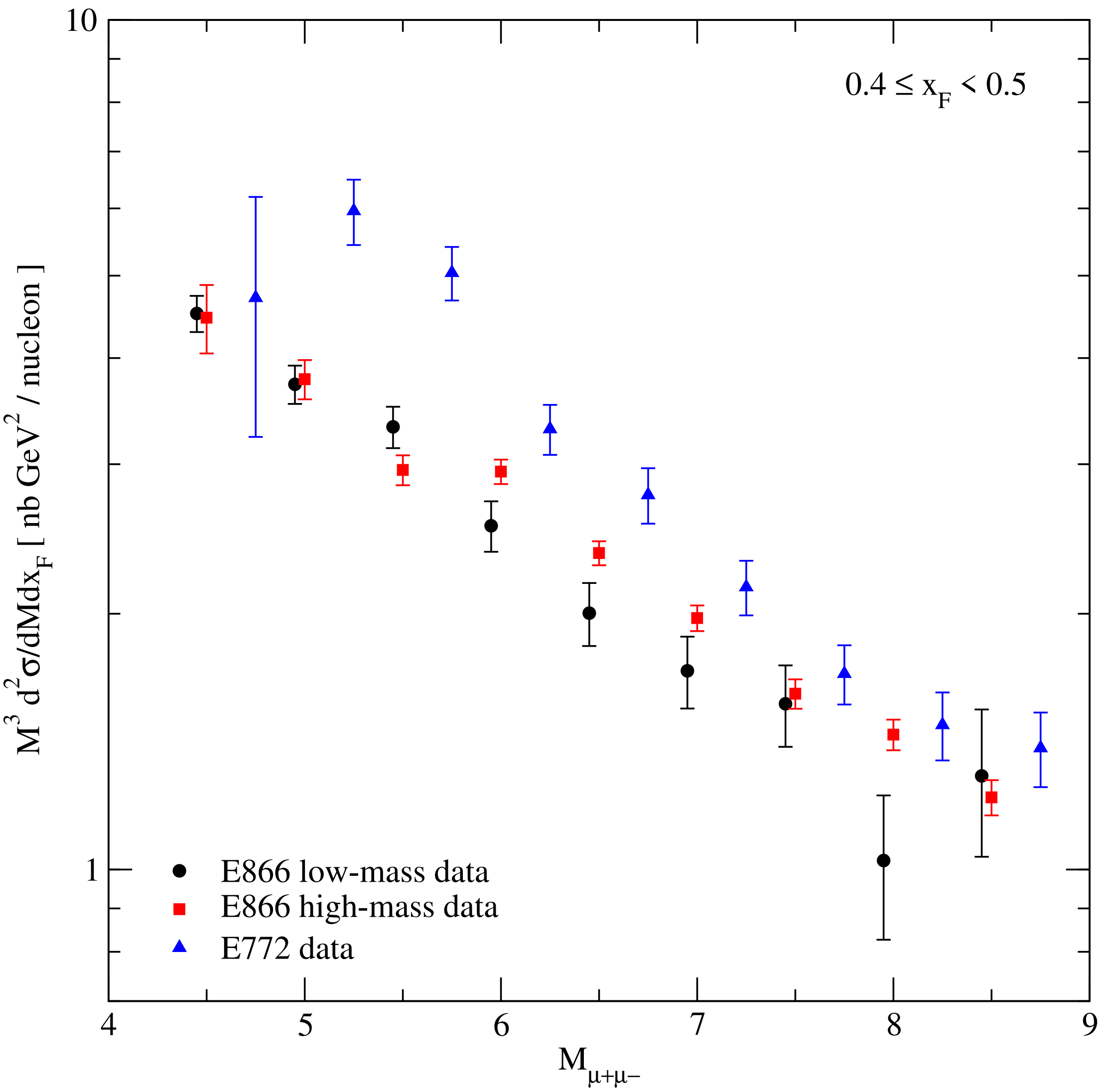

Figure 6.3: A comparison of the results from the low- and high-mass data sets to the E772 results for $0.4 \leq x_F < 0.5$. Error bars represent the statistical uncertainties only, and the high mass data has been offset from the bin center by 0.05 GeV.

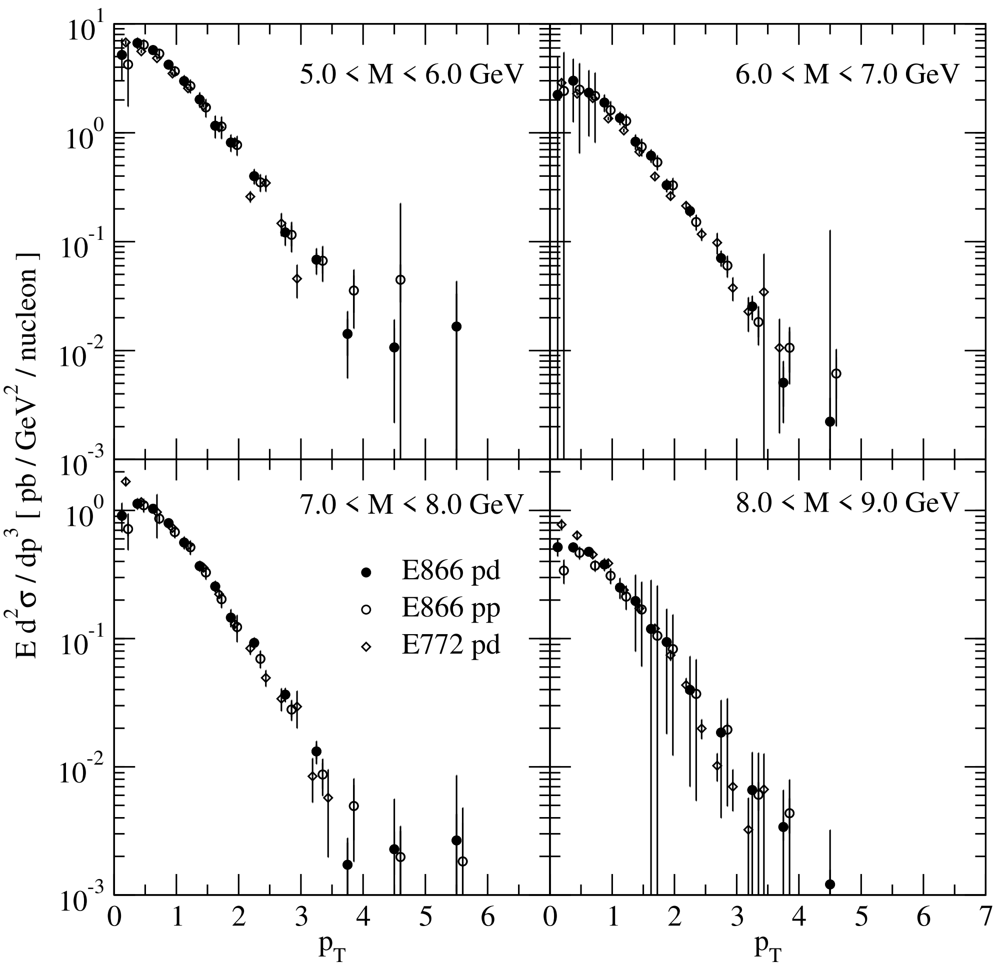

Figure 6.4: Comparison of the E866 measurement of the invariant cross section $Ed^3\sigma/dp^3$ in pd (closed circles) and pp (open circles, offset by 0.1 GeV) interactions to the E772 pd (open diamonds, offset by 0.05 GeV) measurement. The cross sections are in the range $0 \leq x_F < 0.3$. The E866 error bars are the linear sum of the statistical and systematic uncertainties.

the deuterium-to-hydrogen cross section ratio as a function of x_2, which provides a clean probe of the Björken-x dependence of the ratio of anti-down to anti-up quarks in the nucleon sea[3]. Those results [Haw 98, Tow 01] have already been published and incorporated into the various global analyses of the parton distribution functions [CTEQ, MRST, GRV].

Although the previous analysis and this current work began with the same data sample, the tighter event selection criteria required for absolute normalization resulted in the elimination of much of the data above $x_2 \approx 0.15$. Direct comparison between the results presented in chapter 5 and those of Towell *et al.* [Tow 01] are complicated by this. Further complicating matters, the results of Towell *et al.* are differential only in a single variable (x_2)[4], while our new results are differential in the mass and x_F of the dimuon pair.

In figure 6.5, we present the deuterium-to-hydrogen cross-section ratio versus mass in four x_F bins. The ratios were calculated by integrating the data in tables 5.3 through 5.10 over all p_T and taking the ratio of deuterium to hydrogen in each bin. Next-to-leading order calculations of the cross section ratio, based on the CTEQ 5 and CTEQ 6[5] parton distributions, are also shown in the figure. Since

---

[3] Although not explicitly shown in chapter 1, the ratio of the leading-order pd and pp cross sections can be written for large x_F as $\frac{\sigma_{pd}}{\sigma_{pp}}(M, x_F; x_2) \approx \left\{ \frac{1+\frac{1}{4}\frac{d}{u}(x_1)}{1+\frac{1}{4}\frac{d}{u}(x_1)\frac{\bar{d}}{\bar{u}}(x_2)} \right\} \left(1 + \frac{\bar{d}}{\bar{u}}(x_2)\right)$, where x_2 is evaluated according to equation 1.3.

[4] Towell *et al.* did look at the cross section ratio versus other variables, but none which are directly comparable to our double-differential cross sections.

[5] The MRST 98, MRST 2001 and GRV 98 parton distributions give similar results.

the E866 cross section ratios were used in the CTEQ 5 and CTEQ 6 global analyses, they provide a convenient means to check the consistency between the two analyses. We also superimpose the previous cross section ratio results of Towell *et al.* on figure 6.5. Although those results are differential only in x_2, reference [Tow 01] does quote a mean mass and x_F in each x_2 bin. We therefore plot the cross section ratios in each x_2 bin at the mean mass quoted in the reference, and only in the x_F bins appropriate to their mean x_F. Overall, the level of agreement between the data presented in chapter 5 and the cross section ratios previously published by E866 is quite good.

To provide a more detailed and direct comparison with the previously published results, we calculated the absolute cross section $d^2\sigma/dx_1dx_2$ for hydrogen and deuterium using the same x_2 binning as reference [Tow 01] and the same procedures as outlined in chapter 4. For this study, the event selection criteria were loosened to admit the large-x_2 events which were otherwise problematic in the absolute cross sections analysis[6]. Figure 6.7 shows the deuterium-to-hydrogen cross section ratio versus x_2 as calculated in this analysis in three different x_1 bins. As with the previous analysis, there appears to be no significant x_1 dependence on the cross section ratio. Averaging the ratios over all x_1 we obtain a cross section

[6]Specifically, these events tended to occupy regions of the spectrometer with either known efficiency problems or uncertainties in reconstructing the event kinematics. These effects should almost completely cancel in ratio. We did not include any data from intermediate mass data sets 3 and 4, which account for approximately 1/3 of the total number of events used in reference [Tow 01].

ratio versus x_2 only, which is compared with the results of Towell *et al.* in figure 6.7. The only differences between the two analyses are almost completely due to the larger event sample available to reference [Tow 01].

6.3 Data versus Theory

Detailed information on how our data will impact the parton distribution functions must inevitably await their incorporation into future global analyses. It is still useful to compare our results with theoretical calculations of continuum dimuon cross sections. Such comparisons will demonstrate whether the existing sets of parton distributions are consistent with our data in kinematic regions already constrained by previous measurements (E605), and reveal where we expect our data to substantially impact upon the parton distributions in the next round of fits.

As discussed back in chapter 1, continuum dimuon production is sensitive to the gluon distributions through QCD processes at and beyond next-to-leading-order. Dimuon production is dominated by gluon Compton scattering for $p_T > \frac{1}{2}M$ [Ber 98], and the E866 results satisfy this kinematic condition over an extended range in mass and x_F. Thus, in addition to information on the light-antiquark distributions, our data should provide a new and valuable source of information about the gluon distributions. Because this is still an area of ongoing theoretical investigation, in the following discussion we limit ourselves to a

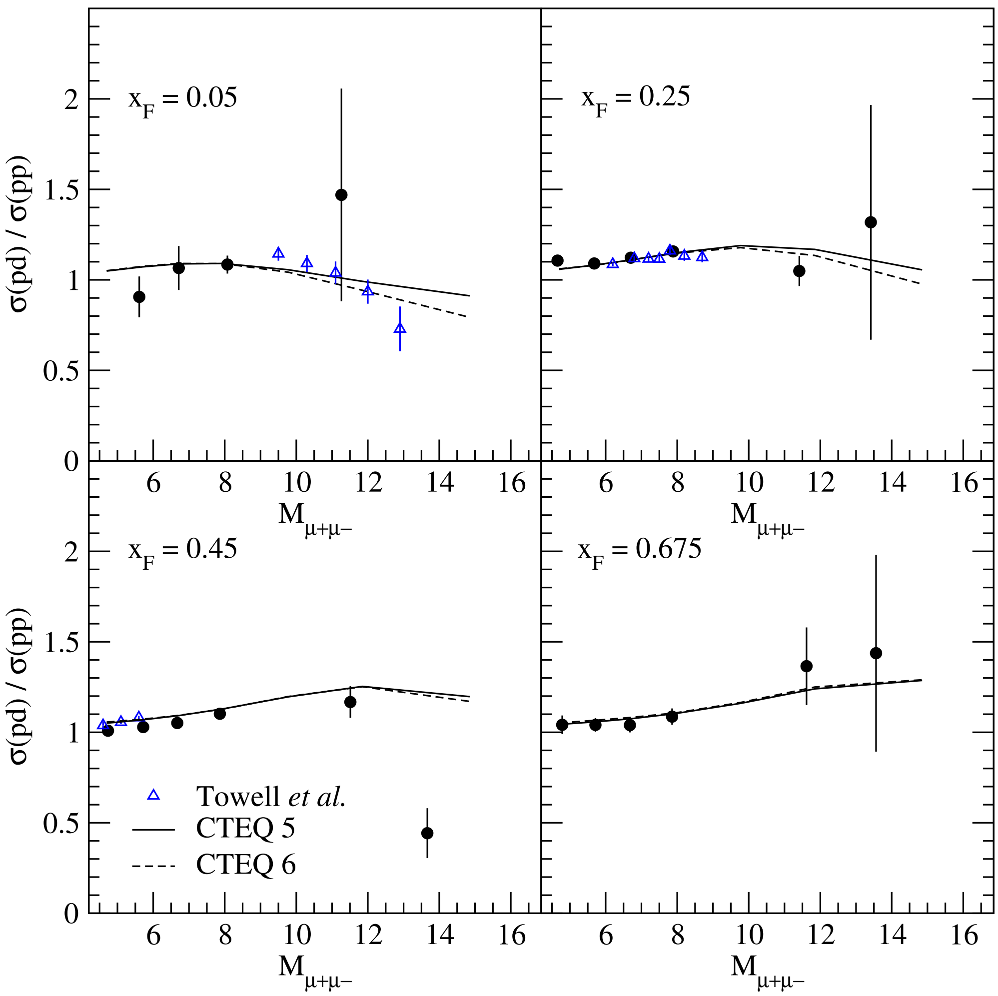

Figure 6.5: Ratio of *pd* and *pp* (per nucleon) cross sections. The results of this analysis (circles) are compared with the results (triangles) of the previous analysis of Towell *et al.* [Tow 01]. Although the results of Towell *et al.* are differential only in x_2, the mean mass and x_F of the events in each x_2 bin was tabulated in the reference. We plot those results at those mean mass values, and only in x_F bins appropriate to the mean x_F. NLO calculations of the ratio based on the CTEQ 5 and CTEQ 6 parton distributions are also shown.

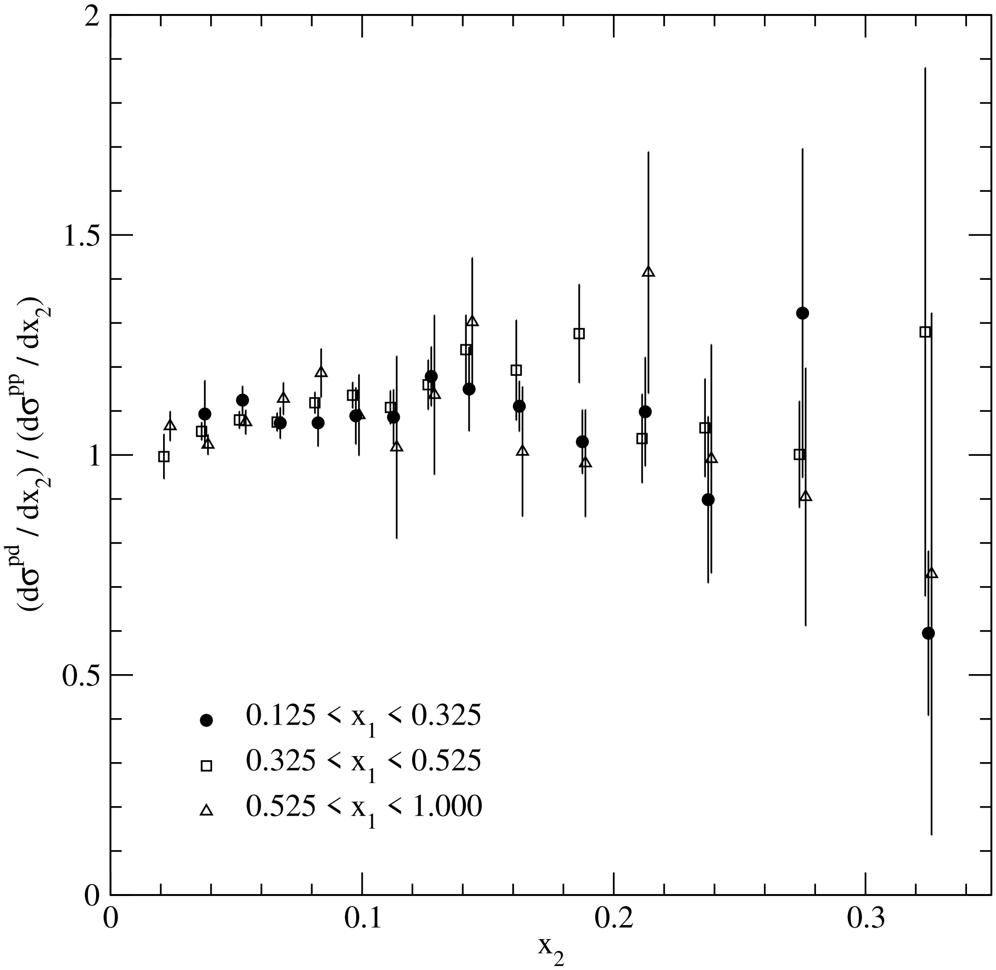

Figure 6.6: Ratio of pd and pp (per nucleon) cross sections plotted versus x_2 in three x_1 bins. The two larger x_1 bins are offset slightly in the horizontal direction from the bin center for clarity.

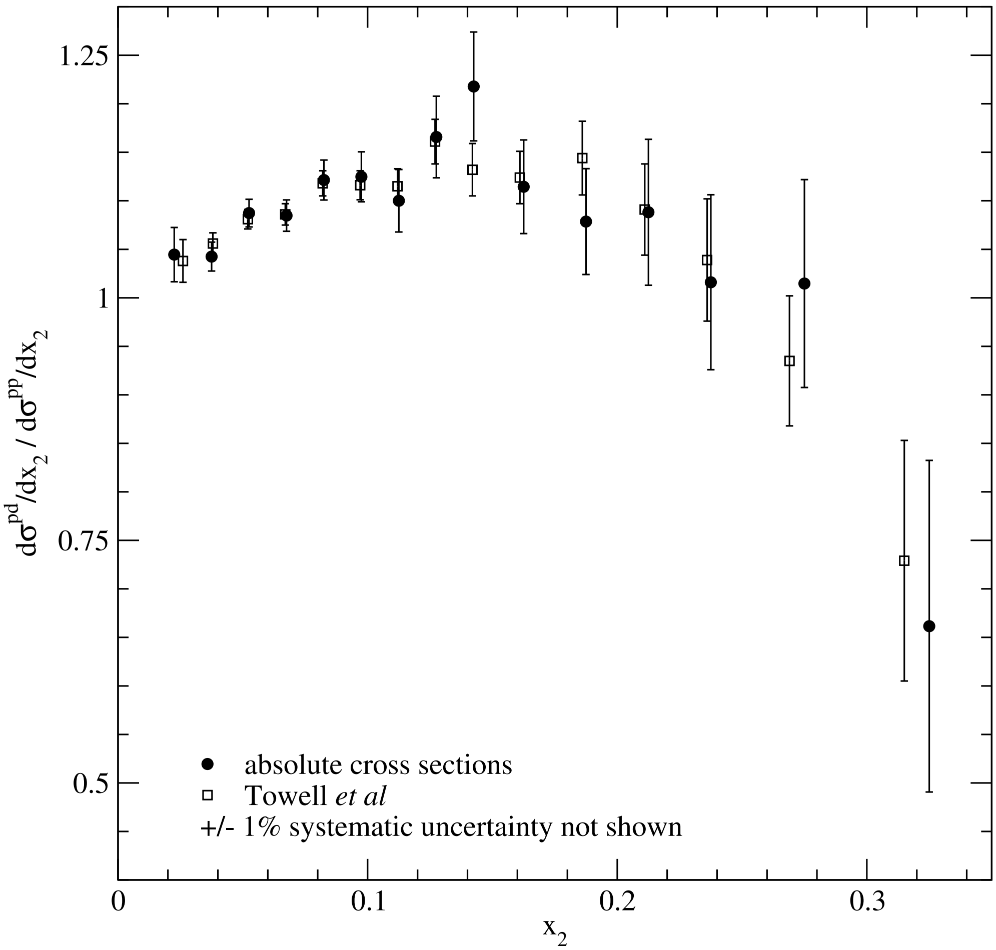

Figure 6.7: Ratio of pd and pp (per nucleon) cross sections plotted versus x_2, at the center of each x_2 bin. The data are compared with the previous E866 results, which are plotted at the mean x_2 in each bin. Both analyses are subject to an additional $\pm1\%$ systematic uncertainty in the relative normalization.

discussion of the quark and antiquark distributions.

6.3.1 Scaling Form: $M^3 d^2\sigma/dMdx_F$

In the preceding chapter, the scaling form $M^3 d^2\sigma/dMdx_F$ was tabulated and plotted in mass and x_F bins. Figures 5.1 through 5.16 plotted the pp and pd cross section in x_F bins versus the invariant mass of the dimuon pair. In each x_F bin we also compared the data to perturbative QCD calculations performed to next-to-leading order. These calculations were based on several of the currently available and most commonly used sets of fits to the parton distributions. In general, they reproduce the shape and normalization of the data well, save for the GRV 98 distributions which systematically overestimate the data by $\sim 20\%$. To better illustrate this, the theoretical calculations were fit to the data to determine a "K'-factor", which we define as the ratio of the experimentally measured dimuon continuum to NLO theory.

The K'-factors for hydrogen and deuterium are shown in table 6.1. All of the parton distributions studied, with the exception of the GRV 98 set, reproduce the normalization of the measured cross sections to better than our systematic uncertainties. This is not unexpected. The valence distributions are well constrained by DIS measurements, and the E605 Drell-Yan data (with which we agree) are an important input into the fits, constraining the antiquark sea over much of the range covered by E866 [CTEQ, MRST, GRV].

Table 6.1: K'-factors, where $K' = \frac{\sigma^{\text{exp}}}{\sigma^{\text{NLO}}}$, for 800-GeV pp and pd dimuon production. The errors represent the statistical and point-to-point systematic uncertainties in the data. The data are subject to an additional $\pm 6.5\%$ uncertainty in the normalization.

PDF	K'_{pp}	χ^2/ndf	K'_{pd}	χ^2/ndf
CTEQ5	0.9753 ± 0.0037	1.47	0.9633 ± 0.0017	2.56
CTEQ6	1.0150 ± 0.0028	1.44	1.0003 ± 0.0004	2.62
MRST 98	0.9732 ± 0.0022	1.43	0.9604 ± 0.0028	2.42
MRST 2001	0.9799 ± 0.0034	1.50	0.9664 ± 0.0078	2.48
GRV 98	0.8107 ± 0.0043	2.11	0.8075 ± 0.0002	4.24

It is interesting to note the improvement in the normalization of the CTEQ 6 [CTEQ 02] based calculations relative to CTEQ 5 [CTEQ 99]. The main difference between the CTEQ 6 distributions and the previous CTEQ fit is a stiffer large-x gluon, the result of including Tevatron jet data in the newer analysis [CTEQ 02]. The same data has also been incorporated into the latest MRST fit [MRST 01], but without as significant a change in the gluon distributions. Though there is improvement in the calculations based on the MRST 2001 distributions over the previous MRST analysis, it is not as dramatic as that seen in the CTEQ distributions.

The relatively poor quality of the fits shown in table 6.1 can be explained by behavior observed in the cross sections which was not anticipated by the parton distribution functions. The agreement between data and theory is quite good below $x_F \approx 0.3$, which is not surprising given the degree of agreement with the E605 data previously discussed. As x_F increases beyond the range constrained by E605, the agreement between the E866 data and the NLO calculations deteriorates, especially at low mass. While this kinematic range probes smaller values of x_2 than reached in E605, it also probes values of x_1 (the momentum fraction of the annihilating quark in the parton model) where the estimated uncertainties on the valence quark distributions are about $\sim 20\%$. Thus, we expect our data to provide important constraints on both the valence and sea quarks in the next round of fits.

6.3.2 $d^2\sigma/dx_1dx_2$

To explore the impact of our data on future fits in more detail, we now examine the cross sections written in the form $d^2\sigma/dx_1dx_2$. While higher-order QCD processes confuse the interpretation of x_1 and x_2 here, one should recall that almost half of the cross section is due to the leading-order $q\bar{q}$ annihilation for which x_1 and x_2 have their usual meaning. Writing the pp and pd cross sections in the limit of large x_F we have

$$
\begin{aligned}
\frac{d^2\sigma_{pp}}{dx_1dx_2} &\propto \frac{4}{9}u(x_1)\bar{u}(x_2) + \frac{1}{9}d(x_1)\bar{d}(x_2) \\
\frac{d^2\sigma_{pd}}{dx_1dx_2} &\propto \left\{\frac{4u(x_1)+d(x_1)}{9}\right\}\left(\bar{d}(x_2)+\bar{u}(x_2)\right).
\end{aligned}
\tag{6.1}
$$

Thus, the shape of the cross sections relative to theoretical calculations should help us understand the effect of our data on the parton distributions.

In the comparisons between data and theory which follow, the cross sections of the form $d^2\sigma/dx_1 dx_2$ were determined using the same procedures outlined in previous chapters. However, certain limitations are imposed on this analysis by the Monte Carlo event sample, which was generated over a limited range in mass and x_F. Because of this, calculating the acceptance in the lowest-lying x_1-x_2 bins is problematic – the x_1-x_2 bins extend beyond the kinematic limits of the Monte Carlo sample. This mainly affects the data below $x_2 = 0.03$, which partially overlaps the the low-mass, large-x_F data discussed in the previous section.

To study the likely impact of our data on future fits to the antiquark distributions, we examine the behavior of data and theory as a function of x_2, the momentum fraction of the annihilating antiquark in the parton model. After the cross sections differential in the momentum fractions of the interacting partons was determined, the ratio of those cross sections to next-to-leading-order calculations based on the CTEQ 6 [CTEQ 02] partons was calculated in each x_1-x_2 bin. Figure 6.8 shows these ratios in two x_1 bins, each containing roughly the same number of events. The difference in shape (if any) between data and theory versus x_2 appears to be consistent over the two ranges in x_1.

In figure 6.9 we average together the ratios of data and theory over all x_1 bins to obtain the ratio of data to theory as a function of x_2 only. The theoretical

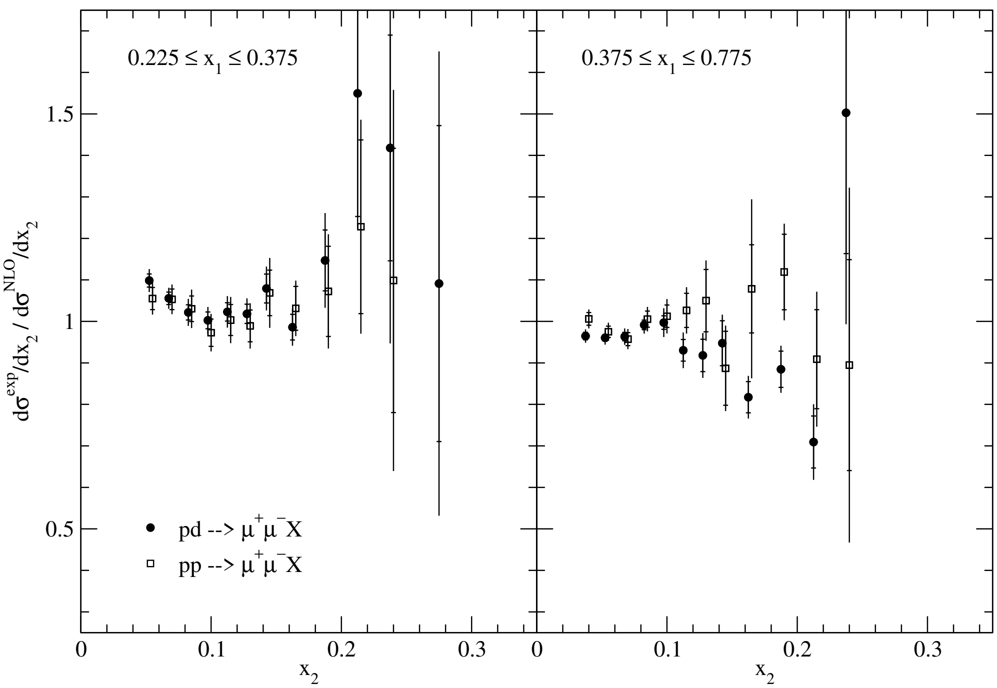

Figure 6.8: Ratio of data to NLO calculations based on CTEQ 6 [CTEQ 02] versus x_2. The left panel shows the range $0.225 \leq x_1 < 0.375$, and the right panel shows the range $0.375 \leq x_1 < 0.775$.

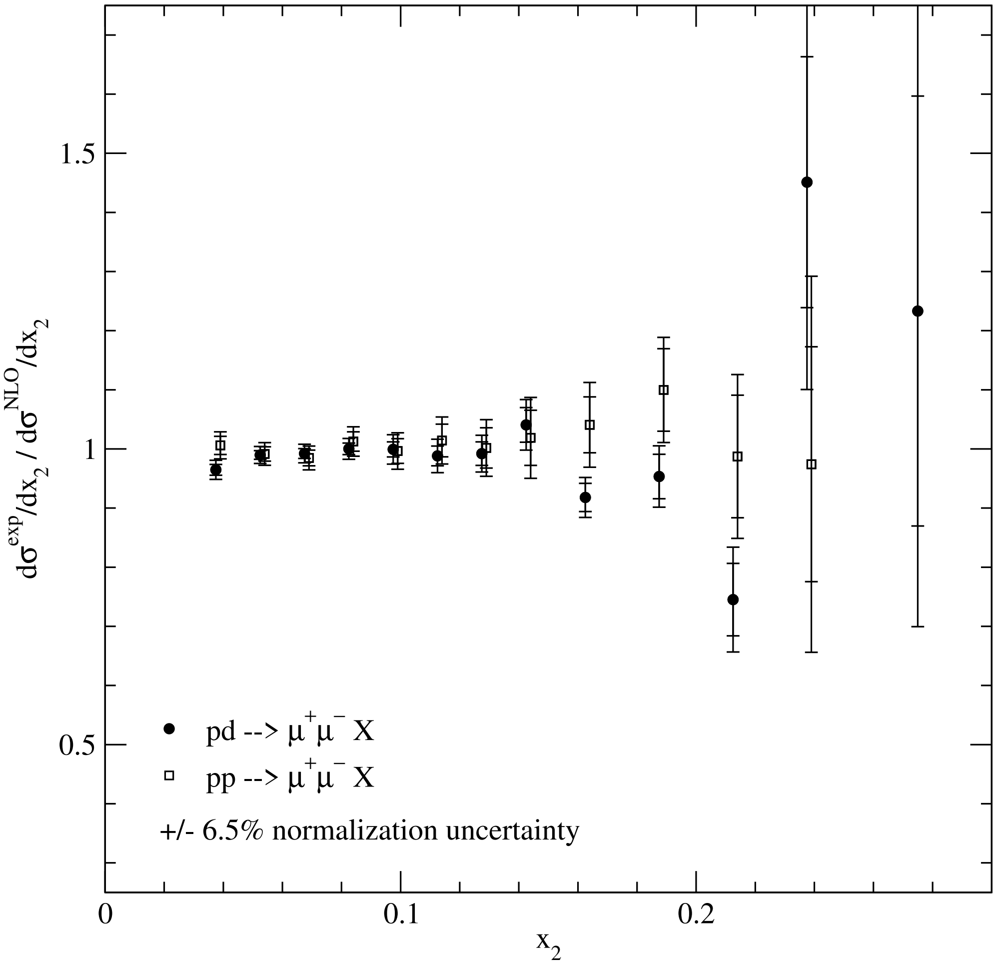

Figure 6.9: Ratio of data to NLO calculations based on CTEQ 6 [CTEQ 02] versus x_2.

calculations clearly reproduce our data well, to within the quoted statistical and systematic errors in the data, over the x_2 range covered. This indicates that the CTEQ 6 fits to the light antiquarks are consistent with our data. Since these fits are largely constrained by the E605 Drell-Yan measurements, this result was not unexpected.

The same analysis can be carried out to examine what our data imply for future fits to the valence quark distributions. Figure 6.10 shows data-divided-by-theory plotted versus x_1, over two x_2 ranges each representing about half of the available statistics. There is an x_1 dependence which is consistent in both x_2 bins. Combining the results over all x_2 in figure 6.11 we see that at large x_1 the data falls about 20% below the theoretical predictions. This seems to suggest that the valence quark distributions are smaller at large Björken-x than in current parton distributions, though not outside the estimated uncertainties of the fits [CTEQ 02]. Parton distribution fits to DIS data at next-to-next-to-leading-order have also recently become available [MRST 02], and they also suggest a reduced valence distribution, relative to current NLO fits.

6.4 Future Prospects

Continuum dimuon production has been an active area of reseach for over thirty years, and the outlook for future measurements remains bright. Based on the cross section ratios published by E866 [Haw 98, Tow 01], Fermilab has accepted a proposal [E906] for a new dimuon experiment, Fermilab Experiment 906, to be conducted using the 120-GeV proton beam from the Main Injector. Like E866, the E906 measurements will examine the differences in continuum dimuon production in pp and pd interactions. Their primary goal is to measured $\frac{\bar{d}}{\bar{u}}(x)$ out to $x \approx 0.5$. The extended range in x is made possible in large measure due to the seven-fold increase in cross section using 120-GeV protons relative to 800-GeV protons.

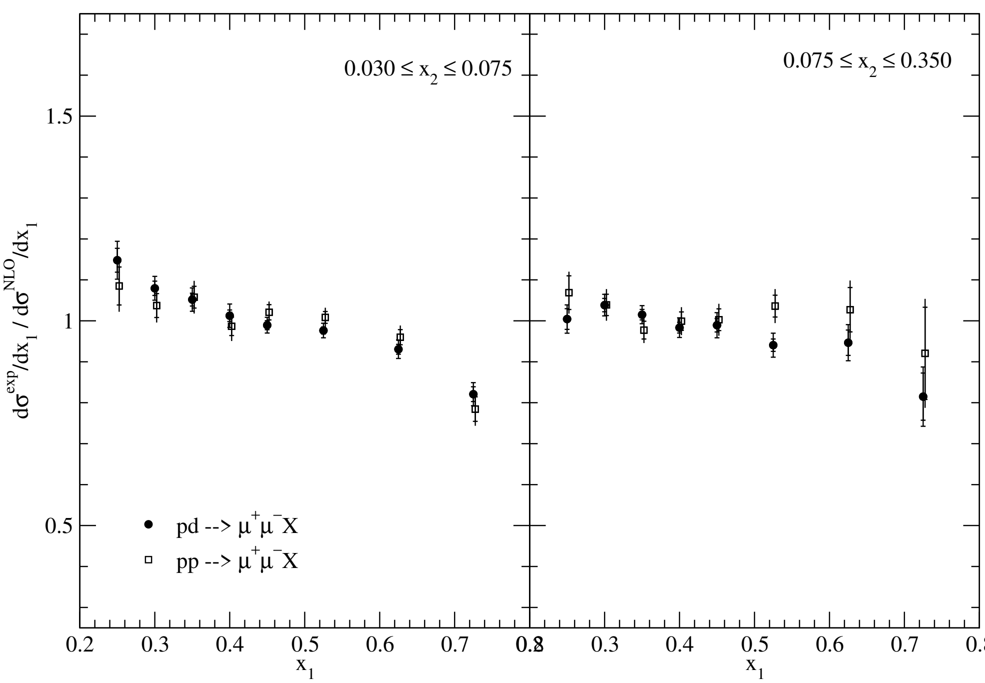

Figure 6.10: Ratio of data to NLO calculations based on CTEQ 6 [CTEQ 02] versus x_1. The left panel shows the range $0.225 \leq x_2 < 0.375$, and the right panel shows the range $0.03 \leq x_2 < 0.350$.

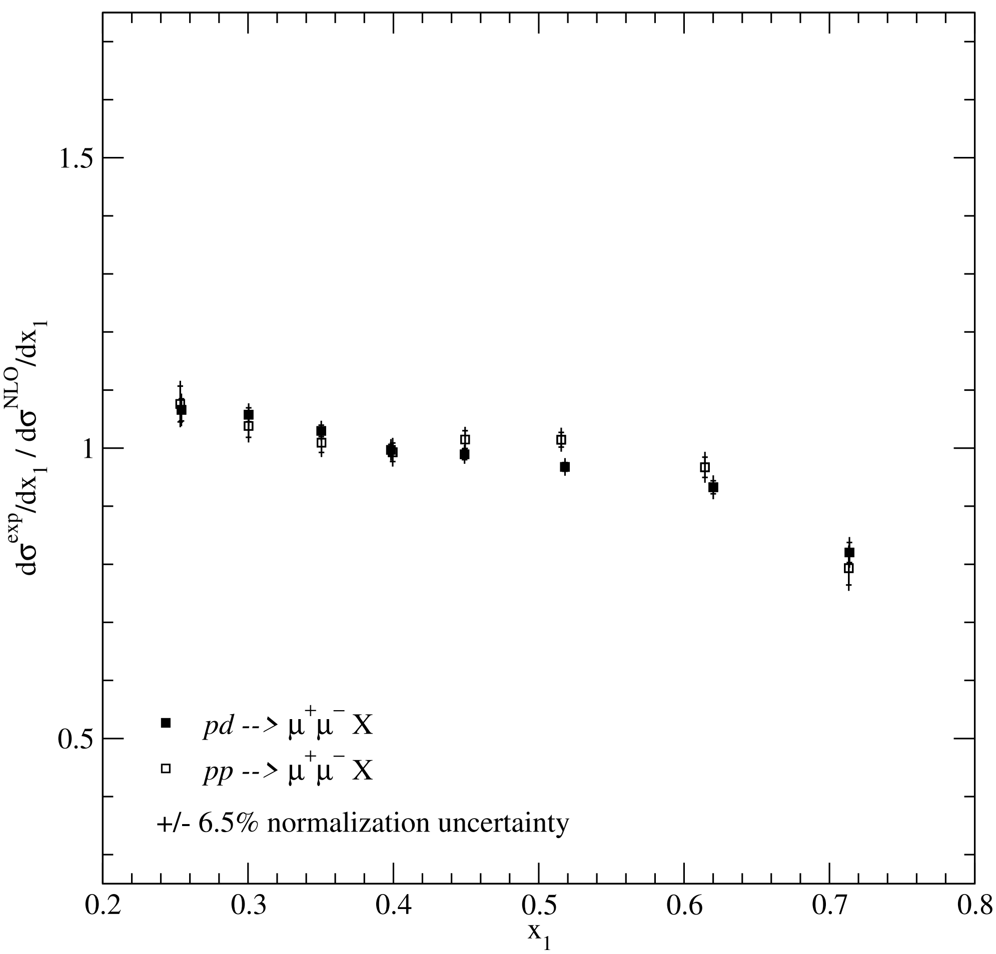

Figure 6.11: Ratio of data to NLO calculations based on CTEQ 6 [CTEQ 02] versus x_1.

Flavor asymmetry is but one of the topics to be adressed with the new experiment. Absolute measurements of the hydrogen and deuterium cross sections will also be possible, greatly extending the kinematic range and statistical precision available to constrain the parton distributions. Furthermore, these measurements may also be able to demonstrate an important property of QCD. Logarithmic scaling violations have long been established in DIS measurements, but have not been conclusively shown using the Drell-Yan process. The reasons for this include the relatively high q^2 probed in dimuon experiments, and the partial cancelation of the effect between the large-x behavior of the valence quarks, and the low-x behavior of the antiquarks [Fre 90, McG 99]. Given the statistical precision and overall understanding of systematic uncertainties attained with the E866 results, comparisons with the future measurements of E906 may well be able to demonstrate scaling violations in the Drell-Yan process.

6.5 Conclusion

Fermilab Experiment 866 has performed an absolute measurement of dimuon cross sections in 800-GeV pp and pd interactions. These data represent the most extensive measurement of the Drell-Yan process to date, covering a wider range of kinematics with better statistical precision than has been achieved in previous measurements. The results are in good agreement with existing pA and pd measurements, as well as NLO calculations based on the various sets of parton distribution functions. The overall level of agreement between data and theory indicates that the antiquark distributions are well understood over the kinematic range relevant to E866. However, differences between data and theory suggest that the valence distributions are overestimated at large x in current parameterizations. Given the statistical precision of the data, we can expect a major impact on future fits to the valence quarks.

REFERENCES

[Ada 95] M.R. Adams et al., Phys. Rev. Lett. **75**, 1466 (1995).

[Ald 90] D.M. Alde et al., Phys. Rev. Lett. **64**, 2479 (1990).

[Ama 91] P. Amaudruz et al., Phys. Rev. Lett. **66**, 2712 (1991); M. Arneodo *et al.* , Phys. Rev. D **50**, R1 (1994).

[Ana 88] E. Anassontzis, et al. Phys. Rev. D **38**, 1377 (1988).

[Ant 82] D. Antreasyan et al., Phys. Rev. Lett. **48**, 302 (1982).

[Bad 83] J. Baider et al., Z. Phys. C **18**, 281, (1983).

[Bal 94] A. Baldit et al., Phys. Lett. B **332**, 244 (1994).

[Bak 84] S.I. Baker *et al.*, Nucl. Inst. Methods A **222**, 467 (1984).

[Ber 98] E. L. Berger, L. E. Gordon and M. Klasen, Phys. Rev. D **58**, 74012 (1998).

[Bet 85] B. Betev *et al.*, Z. Phys. C **28**, 9, (1985).

[Bro 97] C. N. Brown, E866 Internal Memo, September, 1997, *unpublished* .

[Bro 01] C. N. Brown *et al.*, Phys. Rev. Lett. **86**, 2259 (2001).

[Cha 99] T. Chang, New Mexico State University Ph.D. thesis, 1999.

[Chr 70] J.H. Christenson et al. Phys. Rev. Lett. **25**, 1523 (1970), Phys. Rev. D **8**, 2016 (1973).

[Cle 78] J. Cleymans and M. Kuroda, Nucl. Phys. B **155**, 480, (1979) [Erratum-ibid. B **160**, 510 (1979)].

[Cle 79] J. Cleymans and M. Kuroda, Nucl. Phys. B **155**, 480, (1979); Phys. Lett. B **105**, 68 (1981).

[Col 77] J.C. Collins and D.E. Soper, Phys. Rev. D **16**, 2219 (1977).

[Con 89] J. S. Conway et al., Phys. Rev. D **39**, 92 (1989).

[Cor 80] M. Corden *et al.*, Phys. Lett. B **96**, 417 (1980)

[Cri 86] J. A. Crittenden *et al.*, Phys. Rev. D **34**, 2584 (1986); D. E. Jaffe *et al.*, Phys. Rev. D **40**, 2777 (1989).

[CTEQ] See references [CTEQ 99, CTEQ 02]

[CTEQ 99] CTEQ Collaboration, hep-ph/9903282

[CTEQ 02] CTEQ Collaboration, *lookup reference*

[Dre 70] S.D. Drell and T.M. Yan, Phys. Rev. Lett. **25**, 316 (1970).

[E906] The E906 Collaboration, Fermi National Accelerator Laboratory Proposal 906 (unpublished).

[Fre 90] K. Freudenreich, Int. J. Mod. Phys. A **5**, 3643, (1990).

[Haw 98] E.A. Hawker et al., Phys. Rev. Lett. **80**, 3715 (1998).

[Gag 98] C.A. Gagliardi *et al.*, Nucl. Inst. Methods A **418**, 322 (1998).

[GEANT] CN/ASD Group. *Geant – Detector Description and Simulation Tool Q123* CERN, 1993.

[Gin 86] A. Van Ginneken, Nucl. Inst. Methods A **251**, 21 (1986).

[Got 67] K. Gottfried, Phys. Rev. Lett. **18**, 1174 (1967).

[Gre 85] H. B. Greenlee *et al.* Phys. Rev. Lett. **55**, 1555 (1985).

[Gro 00] D. E. Groom *et al.*, The European Physical Journal C **15**, 1 (2000).

[GRV] See reference [GRV 98]

[GRV 98] European Phys. J. C **5**, 461, (1998).

[Kap 78] D. M. Kaplan et al. Phys. Rev. Lett. **40**, 435 (1978).

[McG] P.L. McGaughey (private communication).

[McG 94] P.L. McGaughey et al. Phys. Rev. D **50**, 3038 (1994) [Erratum-ibid. D **60**, 119903 (1999)].

[McG 99] P. M. McGaughey, J.M. Moss, J.C. Peng, Ann. Rev. Nucl. Part. Sci. 49, 217 (1999).

[Mor 91] G. Moreno, *et al.* Phys. Rev. D **43**, 2815 (1991).

[MRST] See references [MRST 98, MRST 01]

[MRST 98] Martin, Stirling, Roberts and Thorne, European Phys. J. C **4**, 463, (1998).

[MRST 01] Martin, Stirling, Roberts and Thorne, European Phys. J. C **23**, 73, (2002).

[MRST 02] Martin, Stirling, Roberts and Thorne, Phys. Lett. B **531**, 216 (2002).

[PAW] CN/ASD Group. *Paw Users Guide, Program Library Q121.* CERN, 1995.

[Pre 02] E. Presley (private communication).

[Ope 94] Vector Fields, LTD. *OPERA-3D Program*, 1994.

[Rod 73] H. M. Roder, G. E. Childs, R. D. McCarty and P.E. Angerhofer, *Survey of the Properties of the Hydrogen Isotopes Below their Critical Termperatures*, National Bureau of Standards Technical Note 641 (1973).

[Smi 81] S. R. Smith et al., Phys. Rev. Lett. **46**, 1607 (1981).

[Tow 99] R. S. Towell, University of Texas at Austin, Ph.D. thesis, 1999.

[Tow 01] R.S. Towell et al., Phys. Rev. D **64**, 052002 (2001).

[Yoh 78] J. K. Yoh et al. Phys. Rev. Lett. **41**, 684 (1978).